Available online at www.sciencedirect.com
SCIENCE DIRECT®
Journal of Solid State Chemistry 177 (2004) 194–201
JOURNAL OF SOLID STATE CHEMISTRY
http://elsevier.com/locate/jssc

Hydrothermal synthesis and structures of the novel niobium phosphates $[NbOF(PO_4)](N_2C_5H_7)$ and $[(Nb_{0.9}V_{1.1})O_2(PO_4)_2(H_2PO_4)](N_2C_2H_{10})$

Xiqu Wang,* Lumei Liu, and Allan J. Jacobson

Department of Chemistry and Center for Materials Chemistry, University of Houston, Houston, TX 77204-5003, USA

Received 15 May 2003; received in revised form 8 July 2003; accepted 12 July 2003

Abstract

Two new niobium phosphates were synthesized and their crystal structures determined from single-crystal X-ray data. $[NbOF(PO_4)](N_2C_5H_7)$ (**1**) (monoclinic, space group $P2_1/c$, $a = 11.442(1)$, $b = 9.1983(7)$, $c = 9.1696(8)$ Å, β=109.94(1)°) has a layered structure and is the first example of a negatively charged $NbOF(PO_4)$ layer analogous to the $MO(H_2O)PO_4$ (M = V, Nb) layers. The layer charge is compensated by interlayer 4-aminopyridnium cations that adopt an unusual arrangement as a consequence of H-bonding and $\pi-\pi$ interactions. The interlayer aminopyridnium cations can be exchanged with alkylammonium ions which form bilayers inclined at $\sim 65°$ to the $NbOF(PO_4)$ layer. $[(Nb_{0.9}V_{1.1})O_2(PO_4)_2(H_2PO_4)]$ $(N_2C_2H_{10})$ (**2**) (orthorhombic, space group $Pbca$, $a = 15.821(2), b = 9.0295(9), c = 18.301(2)$ Å) has a disordered three-dimensional structure based on $NbO(PO_4)$ layers cross-linked by phosphate tetrahedra, and has a similar structure to the known vanadium analog $[V_2O_2(PO_4)_2(H_2PO_4)]$ $(N_2C_2H_{10})$.

Keywords: Niobium phosphate; 4-aminopyridine; Hydrothermal synthesis; Crystal structure; Intercalation compound; Layered structure

1. Introduction

Layered compounds that provide host lattices for intercalation reactions are important for new materials development. The interlayer space serves as a platform in the nanometer regime for tuning properties by topotactic reactions [1–3]. A family of intercalation compounds based on $MOXO_4$ (M = V, Nb, Ta; X = P, As) layers have been intensively investigated [4–7]. $VOPO_4 \cdot 2H_2O$ is one of the best known members of the family. Various organic molecules such as amines and alcohols can be readily intercalated between the formally electroneutral $VO(H_2O)PO_4$ layers [8–10]. The pentavalent vanadium cations can be reduced by redox intercalation reactions, which gives the layers a negative charge that is compensated by intercalated interlayer ions [11,12]. Similar compounds with negatively charged layers due to vanadium atoms of low oxidation state can be prepared also by direct synthesis [13,14]. Hydrated niobium phosphates are closely similar to $VOPO_4 \cdot 2H_2O$ in both structural features and intercalation properties [15]. However, topotactic reduction of the niobium cations is much more difficult. An alternative way to derive charged layers is to replace the coordinated water molecules in the $NbO(H_2O)PO_4$ layer with anionic species. We have reported the intercalation compound $[(NbOPO_4)_4(H_3NCH_2COOH)_2]$ $[H_2PO_4]$ [OH,F] that contains glycinium cations bridging the $NbOPO_4$ layers [16]. Substitution of H_2O_2 [17] and $(PO_4)^{3-}$ for the water molecules were also reported in the literature. In the latter case the layers are linked by interlayer phosphate tetrahedra to form three-dimensional frameworks [18]. In this work we report the first example of a negatively charged $MOF(PO_4)$ layer analogous to $MO(H_2O)PO_4$ layers. Similar layers with the composition $TiF_2(PO_4)$ have been previously reported by Serre and Férey for the compound $TiF_2(PO_4)N_2C_2H_{10}$ [19].

Intercalation materials can be synthesized by reactions of the host lattice directly with the guest molecules.

*Corresponding author. Fax: +1-713-743-2780.
E-mail address: xiqu.wang@mail.uh.edu (X. Wang).

0022-4596/$ - see front matter © 2003 Elsevier Inc. All rights reserved.
doi:10.1016/S0022-4596(03)00400-6

Such reactions usually lead to poorly crystallized products and accurate information on the hybrid structures is difficult to obtain. Crystalline intercalation compounds may be obtained, however, by direct synthesis using hydrothermal techniques [19–22]. We reported recently a number of new niobium phosphates closely related to $NbOPO_4 \cdot nH_2O$. Their crystal structures were determined from X-ray data measured on single crystals that were synthesized hydrothermally [16,23]. Two novel niobium phosphates $[NbOF(PO_4)](N_2C_5H_7)$ (**1**) and $[(Nb_{0.9}V_{1.1})O_2(PO_4)_2(H_2PO_4)](N_2C_2H_{10})$ (**2**) are reported here, both structures are based on the $NbOPO_4$ layers.

2. Experimental

2.1. Synthesis

For the synthesis of compound **1,** a solution was prepared by dissolving 122 mg aminopyridine, 28.5 mg NH_4HF_2 and 0.12 mL 85% phosphoric acid in 2.1 mL H_2O. The solution was sealed together with 20 mg niobium metal in a flexible Teflon bag ($14 \times 2 \times 0.5$ cm) in air. The bag was subsequently sealed in a steel reaction vessel filled with water to about 60% and heated at 160°C for 4 d. After cooling to room temperature in 3 h, the product was filtered off, washed with water, and dried in air. The final pH was ~3. Compound **2** was synthesized in a similar way. A solution was prepared by dissolving 0.05 mL ethylenediamine, 33.3 mg NH_4HF_2 and 0.12 mL 85% phosphoric acid in 2.0 mL H_2O. The solution was sealed together with 15 mg niobium and 15 mg vanadium metal in a flexible Teflon bag ($14 \times 2 \times 0.5$ cm^3) in air. The bag was subsequently sealed in a steal reaction vessel filled with water to about 60% and heated at 160°C for 2 d. The final pH was ~3.

2.2. Characterization

The chemical compositions were analyzed using a JEOL 8600 electron microprobe operating at 15 keV with a 10 μm beam diameter and a beam current of 30 nA.

Thermogravimetric analysis (TGA) for **1** was carried out on a DuPont 2100 TGA system with a heating rate of 5°C/min in air after initially equilibrating the sample at 50°C for 20 min to remove any surface water. Infrared spectra were collected with a Galaxy FTIR 5000 series spectrometer using the KBr pellet method. Powder X-ray data were measured on a Sintag-XDS2000 diffractometer. Preliminary ion-exchange experiments were carried out by stirring 0.1 g powder of compound **1** in 500 mL diluted (0.1 M) alkylammonium chloride solutions for 4 d at room temperatures. After filtration and drying in air the samples were examined by powder X-ray diffraction.

Single-crystal X-ray data were measured on a SMART platform diffractometer equipped with a 1K CCD area detector using graphite-monochromatized Mo$K\alpha$ radiation at 293 K. For each phase a hemisphere

Table 1
Crystal data and structure refinement details

	1	**2**
Formula	$C_5N_2H_7FNbO_5P$	$C_2H_{12}N_2Nb_{0.9}O_{14}P_3V_{1.1}$
Formula weight	318.01	520.65
Temperature (K)	293(2)	293(2)
Wavelength (Å)	0.71073	0.71073
Space group	$P2_1/c$	*Pbca*
a (Å)	11.442(1)	15.821(2)
b (Å)	9.1983(7)	9.0295(9)
c (Å)	9.1696(8)	18.301(2)
β (deg)	109.94(1)	90
V (Å^3)	907.2(1)	2614.3(5)
Z	4	8
Absorption coefficient/mm^{-1}	1.523	2.029
θ_{max} (deg)	28.7	28.6
Reflections collected	5336	15440
Independent reflections	2111	3079
R_{int}	0.0356	0.1557
Data/parameters	2111/138	3079/219
Goodness-of-fit on F^2	1.062	0.875
$R_1/wR_2(I>2\sigma(I))$	0.0465/0.0927	0.0492/0.0968
R_1/wR_2 (all data)	0.0749/0.1025	0.1882/0.1297

$R_1 = \sum||F_o| - |F_c||/\sum|F_o|, wR_2 = [\sum(w(F_o^2 - F_c^2)^2)/\sum(wF_o^2)^2]^{1/2}$.

Table 2
Atomic coordinates ($\times 10^4$) and equivalent isotropic displacement parameters ($Å^2 \times 10^3$) for **1**

	x	y	z	U_{eq}
Nb(1)	9243(1)	−1(1)	2173(1)	15(1)
P(1)	9867(1)	2500(1)	−56(2)	9(1)
O(1)	9026(3)	1559(4)	3616(4)	16(1)
O(2)	9279(3)	−1543(4)	612(4)	15(1)
O(3)	9293(3)	−1541(4)	3757(4)	15(1)
F(4)	7435(3)	−312(3)	1411(4)	24(1)
O(5)	9007(3)	1563(4)	537(4)	14(1)
O(6)	940(3)	129(4)	2887(4)	22(1)
N(1)	3183(5)	−1122(8)	3417(8)	54(2)
N(2)	6825(5)	−1917(8)	4198(8)	54(2)
C(1)	4997(7)	−542(7)	2918(8)	40(2)
C(2)	5625(5)	−1661(6)	3929(7)	25(1)
C(3)	4956(6)	−2497(7)	4635(8)	38(2)
C(4)	3770(8)	−316(8)	2702(10)	55(2)
C(5)	3743(7)	−2208(9)	4358(10)	48(2)

U_{eq} is defined as one-third of the trace of the orthogonalized U_{ij} tensor.

Table 3
Atomic coordinates ($\times 10^4$) and equivalent isotropic displacement parameters ($Å^2 \times 10^3$) for **2**

	x	y	z	U_{eq}
Nb(1)	2091(1)	2486(1)	1634(1)	10(1)
V(1)	2091(1)	2486(1)	1634(1)	10(1)
Nb(2)	−2125(1)	2462(2)	875(1)	10(1)
V(2)	−2125(1)	2462(2)	875(1)	10(1)
P(1)	2576(2)	5075(3)	359(1)	7(1)
P(2)	2445(2)	39(3)	2866(1)	9(1)
P(3)	38(2)	3408(3)	1080(1)	12(1)
O(1)	−1949(4)	1036(6)	1704(3)	9(2)
O(2)	1827(4)	960(7)	2399(3)	10(2)
O(3)	2012(4)	4060(7)	828(3)	12(2)
O(4)	−1969(4)	3945(7)	77(3)	10(2)
O(5)	3137(4)	2331(7)	1633(3)	16(2)
O(6)	657(4)	2758(7)	1614(3)	11(2)
O(7)	−3152(4)	2448(8)	891(3)	17(2)
O(8)	−691(4)	2405(7)	886(3)	9(1)
O(9)	−1902(4)	4125(7)	1605(3)	10(2)
O(10)	1829(4)	977(6)	849(3)	9(2)
O(11)	−1863(4)	860(7)	154(3)	10(2)
O(12)	1998(4)	4050(7)	2401(3)	8(2)
O(13)	−315(4)	4915(7)	1400(3)	19(2)
O(14)	507(4)	3853(8)	361(3)	25(2)
N(1)	−313(5)	270(8)	2120(4)	26(2)
N(2)	463(5)	−2371(9)	687(4)	22(2)
C(1)	−78(7)	−1226(10)	1773(4)	24(2)
C(2)	70(7)	−986(10)	967(5)	23(2)

U_{eq} is defined as one-third of the trace of the orthogonalized U_{ij} tensor.

Table 4
Selected bond lengths (Å) for **1**

Nb(1)–O(6)	1.829(3)
Nb(1)–F(4)	1.966(3)
Nb(1)–O(3)	2.016(3)
Nb(1)–O(1)	2.023(3)
Nb(1)–O(2)	2.026(3)
Nb(1)–O(5)	2.029(3)
O(6)–Nb(1)–F(4)	175.4(2)
O(6)–Nb(1)–O(3)	91.3(2)
F(4)–Nb(1)–O(3)	85.5(1)
O(6)–Nb(1)–O(1)	94.1(2)
F(4)–Nb(1)–O(1)	89.2(1)
O(3)–Nb(1)–O(1)	90.4(1)
O(6)–Nb(1)–O(2)	91.4(2)
F(4)–Nb(1)–O(2)	85.4(1)
O(3)–Nb(1)–O(2)	90.8(2)
O(1)–Nb(1)–O(2)	174.4(1)
O(6)–Nb(1)–O(5)	94.3(2)
F(4)–Nb(1)–O(5)	89.0(1)
O(3)–Nb(1)–O(5)	174.2(2)
O(1)–Nb(1)–O(5)	88.0(2)
O(2)–Nb(1)–O(5)	90.2(1)
P(1)–O(2)	1.526(4)
P(1)–O(3)	1.530(4)
P(1)–O(1)	1.536(4)
P(1)–O(5)	1.540(4)
O(2)–P(1)–O(3)	106.8(2)
O(2)–P(1)–O(1)	111.1(2)
O(3)–P(1)–O(1)	110.5(2)
O(2)–P(1)–O(5)	110.7(2)
O(3)–P(1)–O(5)	110.8(2)
O(1)–P(1)–O(5)	107.1(2)

of data (1271 frames at 5 cm detector distance) was collected using a narrow-frame method with scan widths of 0.30° in ω and an exposure time of 30 s/frame. The data were integrated using the Siemens SAINT program [24]. An absorption correction was made using the program SADABS [25]. The structures were solved by direct methods and refined using SHELXTL [26]. The F atom sites were distinguished from O atoms by using bond valence calculations [27] and by the refined displacement parameters that were found to define unreasonably small thermal ellipsoids if the scattering parameters of oxygen instead of fluorine were used. The ratio of the Nb to V content for **2** was fixed to the value observed from electron microprobe analysis in the final refinement. Hydrogen atoms were refined isotropically with constraints on atom distances. Crystallographic and refinement details are summarized in Table 1. Atom coordinates are listed in Tables 2 and 3. Selected bond lengths are given in Tables 4 and 5. Crystallographic data have been deposited with the Cambridge Crystallographic Data Center as supplementary publication no. CCDC 206379 and CCDC 206380. Copies of the data can be obtained free of charge on application to CCDC, 12 Union Road, Cambridge CB2 1EZ, UK (Fax: (44)1223336-033; e-mail: deposit@ccdc.cam.ac.uk).

Table 5
Selected bond lengths (Å) and angles (deg) for **2**

NbV(1)–O(5)	1.661(6)
NbV(1)–O(12)	1.996(6)
NbV(1)–O(2)	2.008(6)
NbV(1)–O(10)	2.023(6)
NbV(1)–O(3)	2.052(6)
NbV(1)–O(6)	2.284(6)
O(5)–NbV(1)–O(12)	97.7(3)
O(5)–NbV(1)–O(2)	98.6(3)
O(12)–NbV(1)–O(2)	88.9(2)
O(5)–NbV(1)–O(10)	98.4(3)
O(12)–NbV(1)–O(10)	163.8(3)
O(2)–NbV(1)–O(10)	89.4(2)
O(5)–NbV(1)–O(3)	96.8(3)
O(12)–NbV(1)–O(3)	90.6(2)
O(2)–NbV(1)–O(3)	164.5(3)
O(10)–NbV(1)–O(3)	86.8(2)
O(5)–NbV(1)–O(6)	178.3(3)
O(12)–NbV(1)–O(6)	82.1(2)
O(2)–NbV(1)–O(6)	83.0(2)
O(10)–NbV(1)–O(6)	81.8(2)
O(3)–NbV(1)–O(6)	81.5(2)
NbV(2)–O(7)	1.626(6)
NbV(2)–O(4)	1.996(6)
NbV(2)–O(11)	2.001(6)
NbV(2)–O(1)	2.009(6)
NbV(2)–O(9)	2.041(6)
NbV(2)–O(8)	2.268(6)
O(7)–NbV(2)–O(4)	98.1(3)
O(7)–NbV(2)–O(11)	102.3(3)
O(4)–NbV(2)–O(11)	88.7(2)
O(7)–NbV(2)–O(1)	96.9(3)
O(4)–NbV(2)–O(1)	164.8(3)
O(11)–NbV(2)–O(1)	90.3(3)
O(7)–NbV(2)–O(9)	99.6(3)
O(4)–NbV(2)–O(9)	88.0(3)
O(11)–NbV(2)–O(9)	158.1(3)
O(1)–NbV(2)–O(9)	87.3(2)
O(7)–NbV(2)–O(8)	177.6(3)
O(4)–NbV(2)–O(8)	84.2(2)
O(11)–NbV(2)–O(8)	77.4(2)
O(1)–NbV(2)–O(8)	80.8(2)
O(9)–NbV(2)–O(8)	80.7(2)
P(1)–O(4)	1.530(7)
P(1)–O(10)	1.533(6)
P(1)–O(3)	1.540(6)
P(1)–O(11)	1.544(6)
O(4)–P(1)–O(10)	112.5(4)
O(4)–P(1)–O(3)	105.8(4)
O(10)–P(1)–O(3)	110.2(3)
O(4)–P(1)–O(11)	111.1(4)
O(10)–P(1)–O(11)	107.0(4)
O(3)–P(1)–O(11)	110.3(4)
P(2)–O(12)	1.516(6)
P(2)–O(1)	1.532(6)
P(2)–O(9)	1.536(6)
P(2)–O(2)	1.542(6)
O(12)–P(2)–O(1)	105.7(4)
O(12)–P(2)–O(9)	111.3(4)
O(1)–P(2)–O(9)	110.0(4)
O(12)–P(2)–O(2)	112.0(4)
O(1)–P(2)–O(2)	111.4(4)
O(9)–P(2)–O(2)	106.5(4)
P(3)–O(6)	1.502(6)
P(3)–O(8)	1.509(6)
P(3)–O(14)	1.564(7)
P(3)–O(13)	1.583(7)
O(6)–P(3)–O(8)	114.6(3)
O(6)–P(3)–O(14)	109.8(4)
O(8)–P(3)–O(14)	108.6(4)
O(6)–P(3)–O(13)	109.0(4)
O(8)–P(3)–O(13)	109.5(4)
O(14)–P(3)–O(13)	104.9(4)

3. Results and discussion

3.1. Synthesis and characterization

Colorless plates of **1** with uniform sizes of $\sim 0.11 \times 0.11 \times 0.01\,mm^3$ were recovered together with residual niobium metal. The yield is about 20% based on niobium. Green square plates of **2** were obtained as a minor phase. Other phases in the product are unidentified colorless and poorly crystallized green powders and residual metals. The yield is $<1\%$ based on Nb. Efforts to improve the purity and yield by changing the starting composition and temperature were unsuccessful. The low yields are typical of reactions that use bulk Nb metal as a starting reactant although high quality single crystals were readily obtained.

The measured atomic ratios by electron microprobe analysis, averaged over the results from 10 crystals of each phase, are Nb:P:F = 1.0:1.0:0.7 for **1** and Nb:V:P = 0.9:1.1:3.0 for **2**, which are consistent with the formulae derived from the structure refinements. The low observed F content for **1** is probably due to the low sensitivity of the method to this element.

TGA data for $[NbOF(PO_4)](N_2C_5H_7)$ (**1**) show that the compound started losing weight at ca. 320°C. A total observed weight loss of 31.8% between 320°C and ca. 800°C agrees with the calculated value of 32.4% by assuming a residual composition of $NbO_{0.5}F(PO_4)$. The residue is amorphous according to powder X-ray data.

Fig. 1 shows the infrared spectrum of compound **1**. Typical stretching vibrations of the pyridinium ring were observed at 1667, 1601 and 1534 cm^{-1}. The characteristic ν(N–H) bands suggest that the pyridine N atom is protonated (3326 and 3216 cm^{-1}) while the NH_2 group remains unprotonated (3416 cm^{-1}). This observation is expected from the corresponding pK_a values 9.11 and 1.18 for 4-aminopyridine. The corresponding hydrogen atoms were successfully located from difference maps during structure refinements.

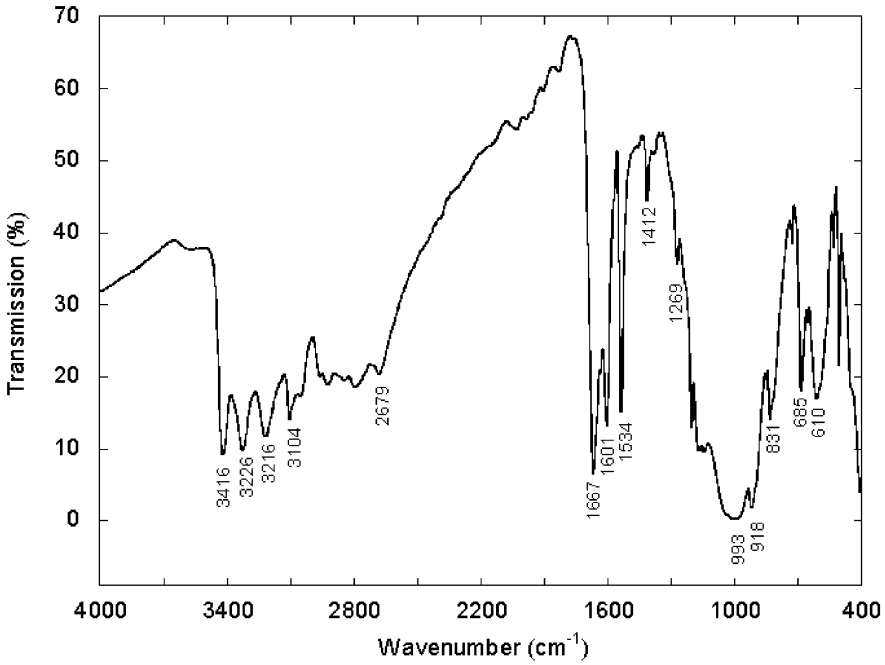

Fig. 1. Infrared spectrum of $[NbOF(PO_4)](N_2C_5H_7)$ (**1**).

3.2. The structure of $[NbOF(PO_4)](N_2C_5H_7)$ (**1**)

The Nb atom has a distorted octahedral coordination with four equatorial Nb–O bonds in the range of 2.016–2.029 Å and two apical bonds Nb–O of 1.829 Å and Nb–F of 1.966 Å. Neighboring NbO_5F octahedra are bridged by the PO_4 tetrahedra in their equatorial plane via sharing of corners to form the typical $MOXO_4$ layer with the F atoms located on both sides of the layer. The layers are stacked along *a*-axis with the interlayer space occupied by the aminopyridinium ions (Fig. 2). Strong hydrogen bond interactions occur between the protonated pyridine N atoms and the apical O atoms of the NbO_5F octahedra (H···O:1.88 Å, N···O:2.70 Å). The unprotonated NH_2 group form two weaker hydrogen bonds with two bridging oxygen atoms (N···O:3.00–3.01 Å). To facilitate the hydrogen bonds the NbO_5F octahedra are slightly tilted, and the apical Nb–O and Nb–F bonds are not collinear (O–Nb–F:175°). The aminopyridinium ions form parallel pairs with opposite orientations. The two parallel pyridine rings are separated by ca. 3.47 Å, suggesting significant $\pi-\pi$ interactions [28]. Neighboring pairs are perpendicular to each other. Therefore, there are four different orientations of the interlayer aminopyridinium ions, all having a tilting angle of $\sim 70°$ toward the layers (Figs. 2 and 3).

Substitution of a fluorine atom for the water molecule in a $NbO_5(H_2O)$ octahedron substantially weakens the apical Nb═O bond. In **1**, bond valences calculated for the apical Nb–O and Nb–F bonds of the NbO_5F octahedron are 1.25 and 0.77 valence units [27], respectively, suggesting that the terminal oxygen atom is more underbonded than the F atom. As a consequence, a strong hydrogen bond is formed between the protonated pyridine nitrogen atom and the terminal oxygen atom rather than to the fluorine atom. To facilitate both the hydrogen bonding and $\pi-\pi$ interactions the pyridine rings form parallel pairs with opposite orientations. The perpendicular arrangement of the pairs is most likely a consequence of packing effects.

3.3. The structure of $[(Nb_{0.9}V_{1.1})O_2(PO_4)_2(H_2PO_4)](N_2C_2H_{10})$ (**2**)

The structure of **2** is closely similar to the vanadium phosphate analog $(VO)_2(PO_4)_2H_2PO_4 \cdot N_2C_2H_{10}$ (**3**) [20]. Both compounds have a three-dimensional framework structure based on (V,Nb)OPO_4 layers that are bridged by interlayer PO_4 tetradedra (Fig. 4). In compound **3** tetravalent and pentavalent vanadium centers are segregated, which leads to the non-centrosymmetric space group $Pc2_1n$ while in **2** the Nb and V atoms are disordered at both crystallographic sites. Efforts to solve the disorder by refinement of ordered structure models with lower symmetry were unsuccessful. The two metal sites in **2** both have a short apical bond of 1.626–1.660 Å and four equatorial bonds in the range of 1.995–2.051 Å. The other apical bond is rather long (2.271–2.282 Å). Bond valence sums calculated by using parameters for V–O bonds are 3.98 and 4.17 v.u. for *M*1 and *M*2 sites,

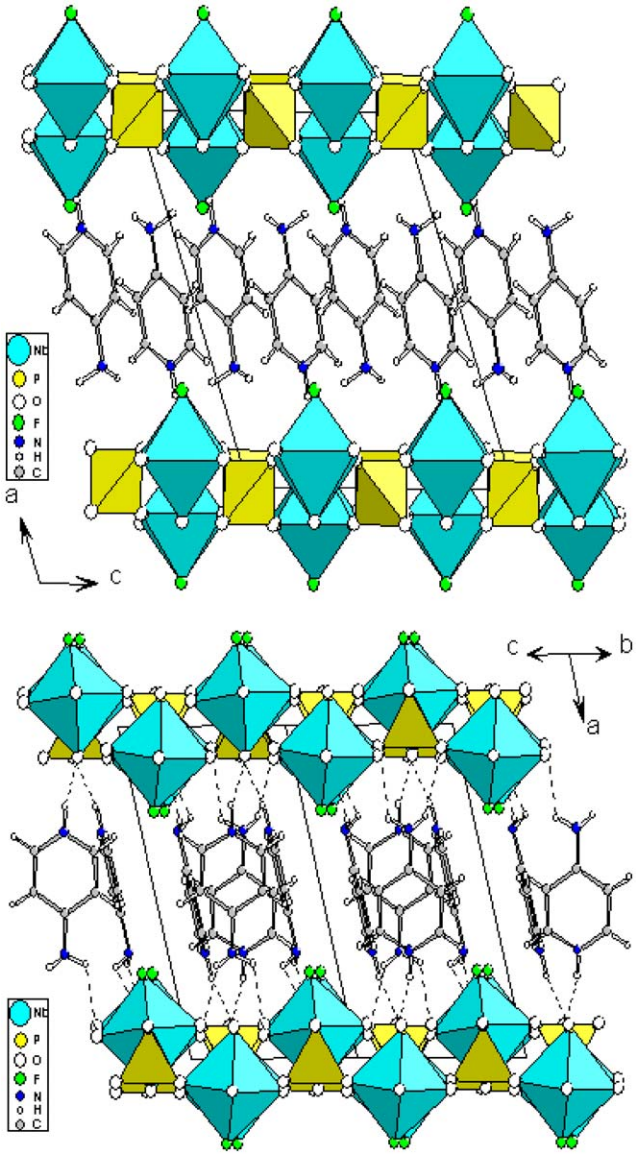

Fig. 2. Views of the structure of **1** along [10] (top) [011] (bottom). Dotted lines represent hydrogen bonds.

respectively, indicating that tetravalent vanadium cations predominate, as expected from the formula. Refined Nb/V ratios are 0.50(1)/0.50 and 0.40(1)/0.60 for the *M*1 and *M*2 sites, respectively. The three-dimensional framework contains irregular channels along [010] and [021] that are occupied by the ethylenediaminium cations. Six strong hydrogen bonds occur between the two NH_3 groups and framework oxygen atoms (N···O:2.79–3.04 Å).

3.4. Ion-exchange of $[NbOF(PO_4)](N_2C_5H_7)$ (**1**)

The aminopyridinium cations of **1** can be ion-exchanged with linear alkylammonium cations. The basal spacing increases linearly with the chain length of

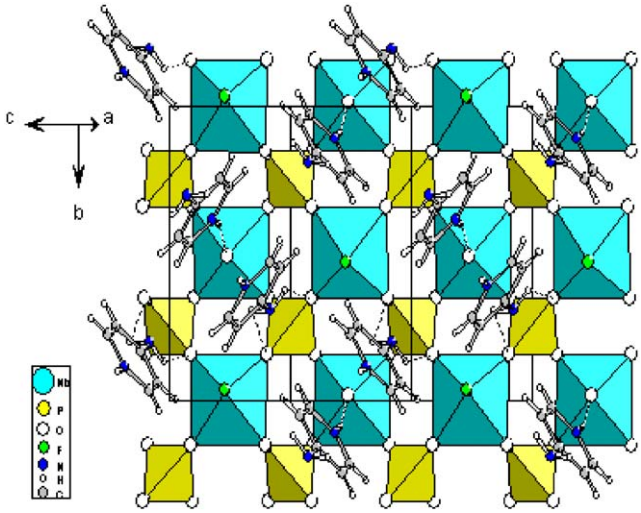

Fig. 3. The arrangement of the interlayer aminopyridinium ions in **1** viewed along [201]. Only one $NbOF(PO_4)$ layer is plotted.

exchanged alkylamines (Fig. 5). The increase of the basal spacing of 2.3 ± 0.1 Å with the increase of one carbon atom in the amines suggests bilayers of alkylammonium chains that are tilted at angles of $\sim 65°$ to the $NbOF(PO_4)$ layer. Similar results were reported for intercalation reactions of $NbOPO_4 \cdot 3H_2O$ [15]. The ion-exchange reactions were incomplete under the experimental conditions used, and the products contain different amounts of the starting material. Products from reactions with ethylammonium and butylammonium ions gave no reliable interlayer spacing data because of low crystallinity.

4. Conclusions

Hydrothermal reactions under mild conditions led to the new niobium phosphates **1** and **2**. Their crystal structures have been obtained from single-crystal X-ray data. Compound **1** represents a unique example of $NbOFPO_4$ layers with a negative charge that is balanced by the interlayer exchangeable organic ions. A related niobium fluorophosphate with a defect $MOXO_4$ layer structure was recently reported which has interlayer Ba^{2+} ions [23]. Compound **2** has a three-dimensional structure that consists of $MOPO_4$ layers interlinked by PO_4 tetrahedra with organic cations filling the channels. A compound with a similar three-dimensional structure but with defective $NbOPO_4$ layers was also synthesized by using Ba^{2+} ions [23]. Differences in F contents and defect patterns lead to different charge distributions among the layers and therefore giving rise to possibilities to incorporate diverse interlayer and interstitial guest species. Further new niobium phosphates with closely related structures are anticipated.

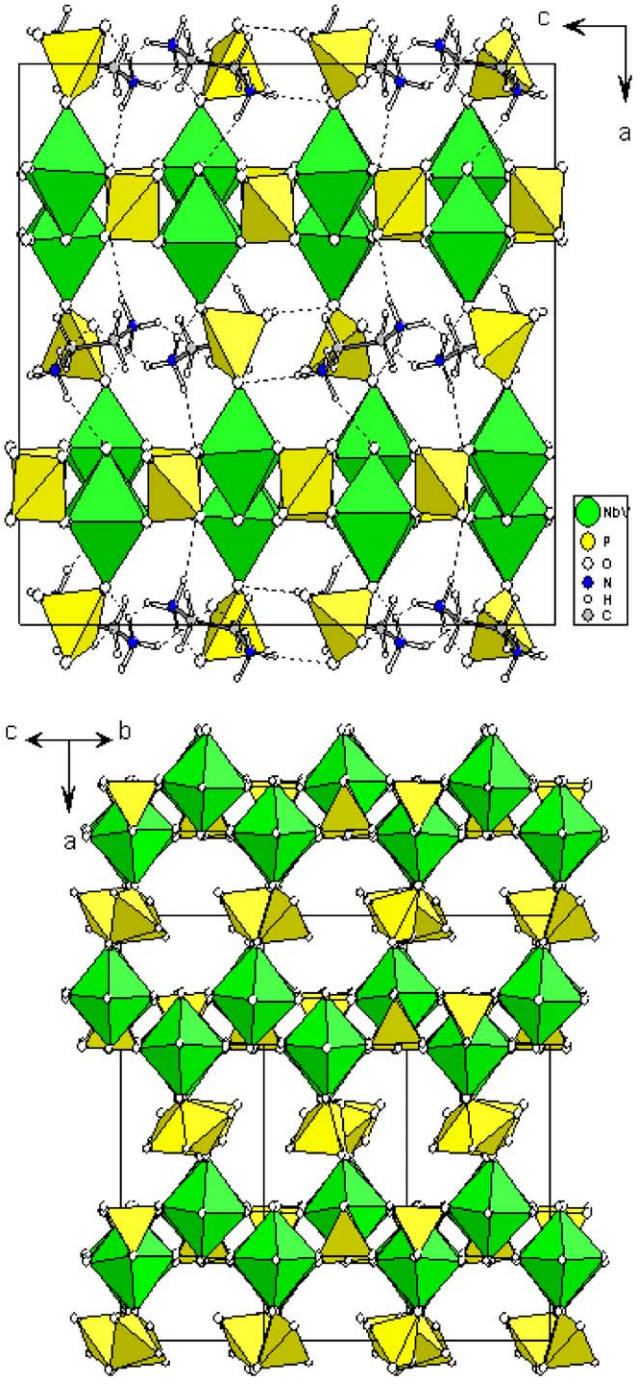

Fig. 4. Views of the structure of **2** along [010] (top) and along [021] (bottom). Interlayer cations are omitted in the latter. Dotted lines represent hydrogen bonds.

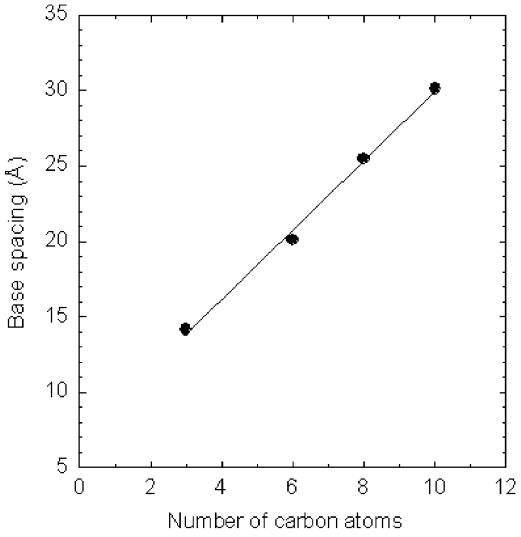

Fig. 5. Change of basal spacing of $[NbOF(PO_4)](N_2C_5H_7)$ (**1**) upon ion exchange with alkylammonium ions ($C_nH_{2n+1}NH_3^+$).

Acknowledgments

We thank the National Science Foundation (DMR-0120463), the R.A. Welch Foundation for financial support. This work made use of Shared Experimental Facilities of the Center for Materials Chemistry (CMC-UH) at the University of Houston.

References

[1] I. Khan, D. O'Hare, J. Mater. Chem. 12 (2002) 3191.
[2] G. Alberti, U. Costantino, Compr. Supramol. Chem. 7 (1996) 1.
[3] A.J. Jacobson, in: A.K. Cheetham, P. Day (Eds.), Solid State Chemistry Compounds, Oxford University Press, New York, 1992, p. 182.
[4] Y.K. Shin, D.G. Nocera, J. Am. Chem. Soc. 114 (1992) 1264.
[5] K. Melanova, K.L. Benes, V. Zima, R. Vahalova, M. Kilian, Chem. Mater. 11 (1999) 2173.
[6] R.F. de Farias, C. Airoldi, J. Solid State Chem. 166 (2002) 277.
[7] N. Yamamoto, N. Hiyoshi, T. Okuhara, Chem. Mater. 14 (2002) 3882.
[8] G. Ladwig, Anorg. Allg. Chem. 338 (1965) 266.
[9] H.R. Tietze, Aust. J. Chem. 34 (1981) 2035.
[10] J.W. Johnson, A.J. Jacobson, J.F. Brody, S.M. Rich, Inorg. Chem. 21 (1982) 3820.
[11] J.W. Johnson, A.J. Jacobson, Angew. Chem. Int. Ed. Engl. 22 (1983) 412.
[12] A.J. Jacobson, J.W. Johnson, J.F. Brody, J.C. Scanlon, J.T. Lewandowski, Inorg. Chem. 24 (1985) 1782.
[13] S.-L. Wang, H.-Y. Kang, C.-Y. Cheng, K.-H. Lii, Inorg. Chem. 30 (1991) 3496.
[14] Y. Zhang, A. Clearfield, R.C. Haushalter, J. Solid State Chem. 117 (1995) 157.
[15] K. Beneke, G. Lagaly, Inorg. Chem. 22 (1983) 1503.
[16] X. Wang, L. Liu, H. Cheng, A.J. Jacobson, Chem. Commun. 1999 (1999) 2531.
[17] L. Moreno-Real, E.R. Losilla, M. Aranda, M. Martinez-Lara, S. Bruque, M. Gabas, J. Solid State Chem. 137 (1998) 289.
[18] N. Kinomura, N. Kumada, Inorg. Chem. 29 (1990) 5217.
[19] C. Serre, G. Férey, J. Mater. Chem. 9 (1999) 579.
[20] W.T.A. Harrison, K. Hsu, A.J. Jacobson, Chem. Mater. 7 (1995) 2004.
[21] Y. Shan, R.H. Huang, S.D. Huang, Angew. Chem. Int. Ed. 38 (1999) 1751.
[22] J. Do, R.P. Bontchev, A.J. Jacobson, J. Solid State Chem. 154 (2000) 514.

[23] X. Wang, L. Liu, A.J. Jacobson, J. Mater. Chem. 12 (2002) 1824.
[24] SAINT, Program for Data Extraction and Reduction, Siemens Analytical X-ray Instruments Inc., Madison, USA, 1996.
[25] G.M. Sheldrick, SADABS, Program for Siemens Area Detector Absorption Corrections, University of Gottingen, Germany, 1997.
[26] G.M. Sheldrick, SHELXTL, Program for Refinement of Crystal Structures, Siemens Analytical X-ray Instruments Inc., Madison, USA, 1994.
[27] N.E. Brese, M. O'Keefee, Acta Crystallogr. B 47 (1991) 192.
[28] C.A. Hunter, J.K.M. Sanders, J. Am. Chem. Soc. 112 (1990) 5525.